Analysis of xylitol – citric acid system forming deep eutectic solvent: Application for dissolving poorly water-soluble drugs. A combination of calorimetric and Raman investigations

Yannick Guinet, Laurent Paccou, Alain Hédoux

Analysis of xylitol – citric acid system forming deep eutectic solvent: application for dissolving poorly water-soluble drugs. A combination of calorimetric and Raman investigations.

Yannick Guinet[a], Laurent Paccou[a] and Alain Hédoux[a]*

[a]Univ. Lille, CNRS, INRAE, Centrale Lille, UMR 8207 - UMET - Unité Matériaux et Transformations, F-59000 Lille, France

*corresponding author: alain.hedoux@univ-lille.fr

Abstract

The phase diagram of the xylitol – citric acid system was determined from microcalorimetry experiments performed on mixtures prepared by co-milling. Raman investigations in the stretching regions of carbonyl and hydroxyl groups have shown a close relationship between the formation of molecular associations between the two molecular species and the drastic negative deviation from ideality for high citric acid content, responsible for obtaining a deep eutectic solvent (DES). It was shown that a great amount of poorly water-soluble drugs (ibuprofen and paracetamol) could be dissolved in that DES, providing a strategy for stabilizing a great amount of amorphous drugs or for obtaining unusual crystalline forms of drugs.

Keywords: milling – low-wavenumber Raman spectroscopy – equilibrium phase diagram – poorly water-soluble drugs – deep eutectic solvent – hydrogen-bonded liquids

1. Introduction

In the pharmaceutical area, most of active molecules are synthesized in the solid-state and more specifically in a crystalline poorly water-soluble form. Despite the thermodynamic stability of the crystalline state, its low bioavailability is a major obstacle to the development of new drugs. Several strategies were considered to overcome this drawback, including preparation of solid dispersions[1-3], co-crystals[4], co-amorphous[5, 6] and confined APIs within mesoporous silica (MPS)[7]. Alternatively, ionic liquids (Ils) have received considerable attention for their capabilities to convert a pure chemical solid in an apparently stable liquid state by mixing in certain ratios[8, 9]. However, the use of ILs as solvents was limited in the pharmaceutical field because of their toxicity[9-11]. Another kind of solvents which share several characteristics and properties with ILs are eutectic mixtures[12] characterized by a melting point temperature well below that of an ideal liquid mixture[13, 14], and are so called deep eutectic solvents (DES). These solvents can be considered as promising excipients[15, 16], due to their biodegradable properties and pharmaceutically acceptable toxicity profile, since many of them are formed in a very simple way from natural products, providing thereby green solvents. Most of DES results from hydrogen bonding between donor (HBD) and acceptor (HBA) components[13, 14]. However, it is not sufficient condiment to obtain DES, since any mixture of alcohols should be a DES. It was recently reported in the case of thymol/menthol DES[17] that the deep character of the eutectic mixture would result from H-bond interactions much stronger in the mixture than in any of the pure components. More generally, specific H-bond interactions are considered to be responsible for the depression of the eutectic point temperature[13, 14, 18]. It is worth noting that detailed investigations on H-bonding in DES are relatively uncommon while H-bonding is recognized to be fundamental to explain the solvent properties of deep eutectic mixtures.

In the pharmaceutical area, DES can be used as drug solubilization vehicles, by dissolving the API in the DES[19], or to enhance the dissolution properties of the API by directly forming a DES from the complexation of an API with a co-former[20]. Citric acid is widely used as model co-former to obtain co-crystals[21, 22], and was also identified as HBA capable of forming DES. It is recognized that sugar alcohols are HBD forming DES by complexation with citric acid[18]. Citric acid / xylitol is one of these mixtures classified as DES despite a lack of information on the solid – liquid phase diagram.

The present work focuses in a first stage on the investigation of the equilibrium phase diagram of citric acid / xylitol system and on the detailed analysis of the H-bond interactions between the pure components for the various compositions of the mixtures. In a second stage, two model poorly water-soluble APIs were dissolved in the DES. Low-wavenumber Raman spectroscopy was used for checking the amorphous character of the formulations and monitoring the stability of amorphous drugs in the formulations.

2. Materials and Methods

Xylitol (XYL, purity > 99 %), citric acid (CA, purity > 99.5 %), ibuprofen S (IBP-S, purity 99%), were purchased from Sigma-Aldrich and paracetamol (PARA, purity > 98 %) from ACROS organics, and used without further purification. No specific drying treatment was applied removing residual water. Molecular structures are shown in figure 1. Mixtures were prepared in the full range of compositions by co-milling at room temperature for 1 hour using a Retsch Mixer Mill MM400 (Haan, Germany). After recovering mixture powder, it was sealed into in spherical pyrex containers or in cylindrical quartz containers (for Raman spectroscopy at low-wavenumber and at higher wavenumber respectively) and in stainless steel pans for microcalorimetry measurements. Dissolving IBP-S and PARA in the eutectic mixture was performed after heating the mixture above 80 °C under stirring.

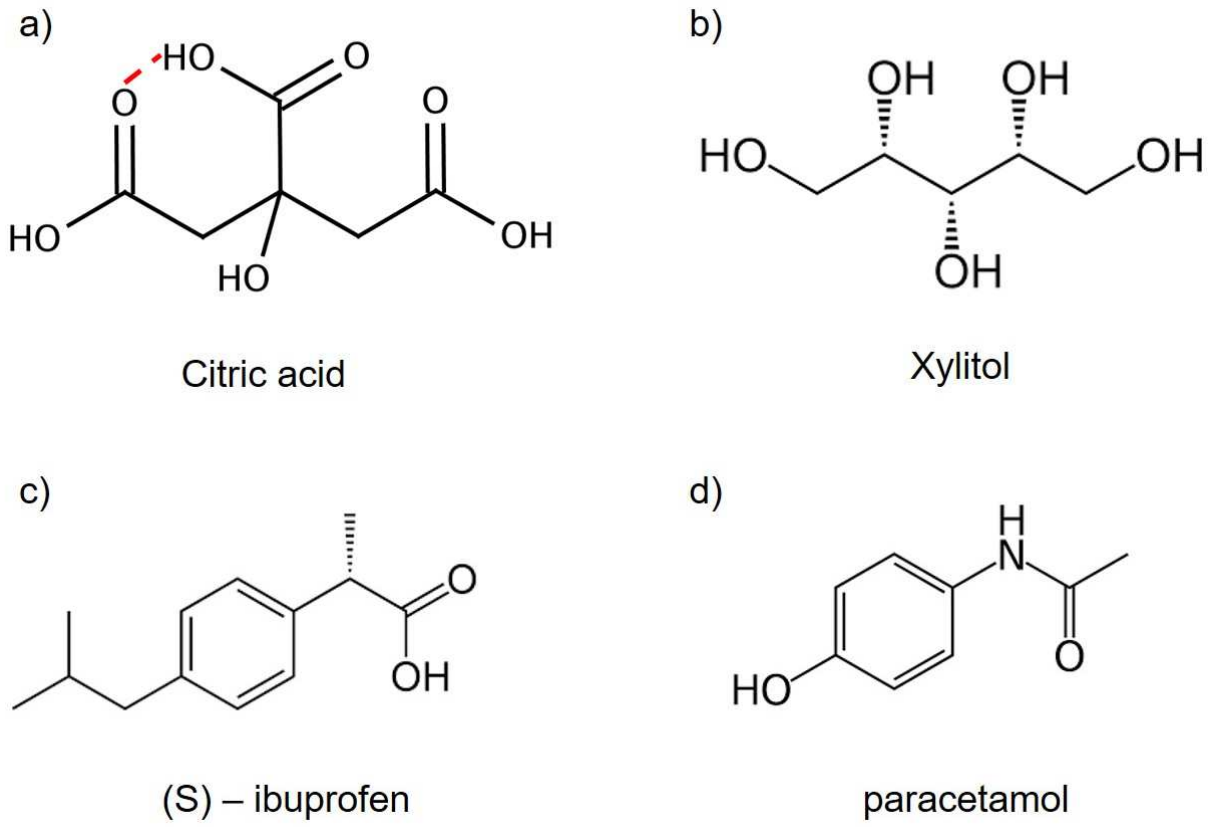

Figure 1: molecular structure of a) citric acid, b) xylitol, c) (S) – ibuprofen, d) paracetamol; the dashed line between oxygen atom and OH group indicates intra molecular H-bonds in citric acid.

Microcalorimetry experiments.

Microcalorimetry measurements were carried out on a very sensitive microcalorimeter microDSC III (Setaram Instrumentation, Caluire, France). Typical sample mass of 300 mg was used for mixtures. Only heating runs were performed with a scanning rate of 0.5 K/min. The temperature

of melting of recrystallized mixtures were determined using Calisto Preprocessing software (Setaram, Instrumentation, Caluire, France). The temperature corresponding to the beginning of the melting of mixtures was determined as the onset of the low-temperature peak, while the temperature corresponding to the end of melting was determined as the endset of the high-temperature peak.

Raman spectroscopy.

Low-frequency investigations were carried out on a high dispersive XY Dilor spectrometer composed of three gratings arranged in a configuration characterized by a focal length of 800 mm. Using the 514.5 nm line of Coherent laser and maintaining the entrance and exit slits opened at 200 µm, allow to collect spectra with an acquisition time of 60s, in the 5 – 600 cm^{-1} spectral range characterized by a resolution lower than 2 cm^{-1}. The temperature of the sample was regulated using an Oxford nitrogen flux device that keeps the temperature fluctuations within 0.1 °C.

Spectra were collected at higher frequencies using an inVia Renishaw spectrometer in backscattering geometry to obtain non-polarized light-scattering spectrum, under a scattering angle θ = 180 °C, using a solid diode laser at 514.5 nm. The quartz cells containing the mixtures were placed in a THMS Linkam temperature device for analyzing the temperature dependence of Raman spectra.

The analysis of the low-wavenumber Raman spectrum requires a specific data processing, widely detailed in several papers[23, 24] and briefly described here after. The Raman intensity was firstly converted into reduced intensity $I_r(\omega)$ by correction of the Bose-Einstein factor. In this representation, the spectrum is dominated by the contribution of the quasielastic scattering (QES) in the very low-wavenumber region (< 70 – 80 cm^{-1}), corresponding to relaxational motions i.e. rapid motions of groups of atoms within the molecule. This contribution is overlapping with the vibrational contribution. This latter contains information about the molecular organization in the short-range order of an amorphous state, while the temperature dependence of the QES is closely connected to order – disorder phase transformations (glass transition, crystallization, polymorphic transformations). To obtain both types of information the two contributions were separated using

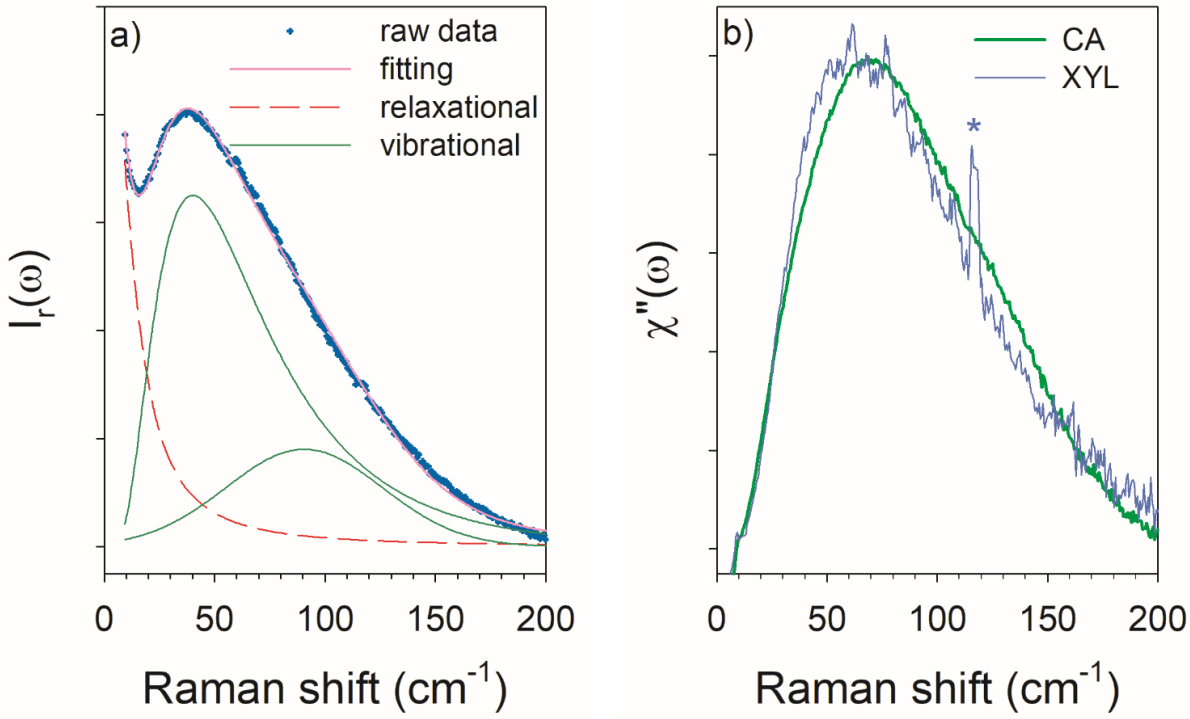

***Figure 2**: Representation of low-wavenumber Raman spectra a) fitting procedure of the reduced intensity spectrum of citric acid at room temperature; b) Raman susceptibility of citric acid (CA), xylitol (XYL) and eutectic mixture (X_{CA} = 0.4) at room temperature. The star localizes a laser line*

the fitting procedure described in figure 2a for the low-wavenumber spectrum of citric acid. The contribution of QES is usually described by a Lorentzian shape centered at ω = 0, and the vibration contribution by a lognormal shape. In order to analyze the phase transformations of molecular materials, the temperature dependence of QES is generally plotted after normalization of the intensity of the Lorentzian by the intensity of the vibrational contribution characterized by a very weak temperature dependence. Additionally, to analyze the molecular organization in highly disordered states, the reduced intensity was converted into Raman susceptibility after the subtraction of the relaxational contribution according to[25, 26]:

$$\chi''(\omega) = \omega . I_r(\omega) = \frac{C(\omega)}{\omega} . G(\omega) \qquad (1)$$

where $\chi''(\omega)$ is the Raman susceptibility, $G(\omega)$ the density of vibrational states (VDOS) and $C(\omega)$ the light-vibration coupling coefficient. The Raman susceptibility of amorphous citric acid is plotted in figure 2b, and compared with amorphous xylitol and eutectic mixture.

3. Results and discussions

3.1.Determination of the phase diagram CA-XYL

In a first step the determination of enthalpy and temperature of melting were performed for pure citric acid (T_m= 154 °C, ΔH_m= 40 kJ/mole), and pure xylitol (T_m= 103 °C, ΔH_m= 38 kJ/mole). Using these data, predictions of the phase diagram by the ideal liquid phase model was plotted (in Figure 3a) from the consideration that the solid-liquid equilibrium lines of each component are described by the equation[27]:

$$\ln(x_i\gamma_i) = \frac{\Delta H_{m,i}}{R}.\left(\frac{1}{T_{m,i}} - \frac{1}{T}\right) \qquad (2)$$

Where x_i, γ_i are the mole fraction and the activity coefficient of the component I, and $\Delta H_{m,i}$, $T_{m,i}$ the enthalpy and temperature of melting. In the frame of the ideal liquid phase model activity coefficients of the two components are set to unit (γ_i = 1).

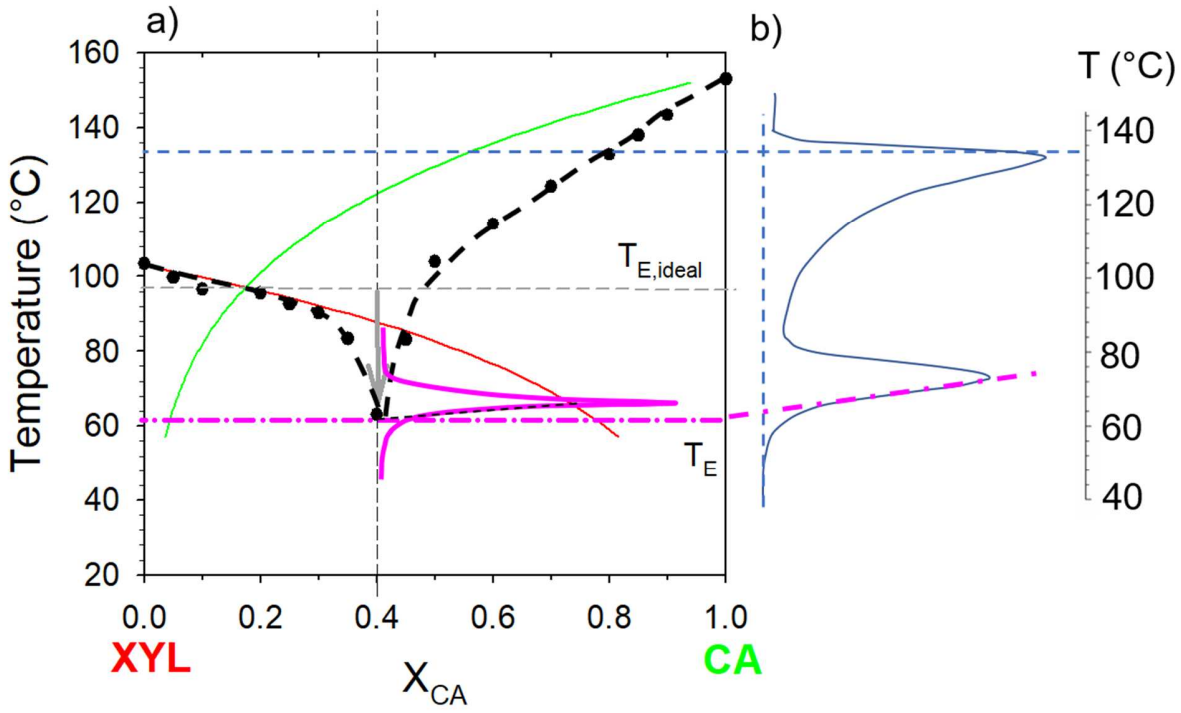

Figure 3: a) experimental solid – liquid equilibrium phase diagram for the system xylitol (XYL) – citric acid (CA) corresponding to full circles and dashed lines; full lines correspond to the ideal solid-liquid lines calculated from equation (2). The arrow shows the temperature depression from the ideal temperature ($T_{E,ideal}$) down to the real temperature (T_E) of the eutectic mixture indicated by the endotherm determined at X_{CA}=0.4; b) the DSC trace of the X_{CA}=0.8 is plotted on the right side of the diagram. The dashed line in the thermogram indicates the temperature of the beginning of melting corresponding to the eutectic temperature (TE) located by the same dashed line in the phase diagram.

Co-milling was used to prepare the mixtures for the microcalorimetry analysis from the consideration that this process promotes the formation of co-crystals[22, 28-30], and thus the formation of supramolecular molecular entities especially co-crystals containing citric acid. DSC

traces obtained for mixtures significantly different from the eutectic composition, plotted in Figure 3b (X_{CA} = 0.8) are typical of those usually obtained for mixtures with eutectic[31]. The eutectic composition (X_{CA}=0.4) is characterized by a sharp endothermic peak of melting. It is worth noting that the negative deviation from ideality is mainly inherent to the deviation from ideality of the CA component. Thermograms obtained for different mixture compositions covering the entire phase diagram are plotted in figure S1 (Supplementary material).

3.2.Raman spectroscopy of CA-XYL mixtures

3.2.a The O – H stretching region was investigated by collecting spectra between 2600 and 3800 cm^{-1}. Spectra of pure amorphous xylitol and citric acid are plotted in Figure 4a after renormalization by the integrated intensity of C – H stretching bands. The O – H stretching spectrum of xylitol is composed of two bands determined by fitting with the residue method, and plotted in dashed lines in Figure 4a. The spectrum of citric acid is also composed of two bands much more splitted than in the spectrum of xylitol. Additionally, the O – H spectrum of citric acid is dominated by an intense low-wavenumber component which can be partly assigned to intramolecular C = O…H – O H-bonds (represented by the dashed line in figure 1a). Indeed, intramolecular H-bonds are expected to be stronger than intermolecular H-bonds, and then detected at lower wavenumbers. Intermolecular H-bonds in CA can be formed between any C=O and O-H groups within the molecule. It cannot be excluded, however, that intermolecular H-bonding gives a contribution to this low-wavenumber band that could explain its strong integrated intensity. The spectra of xylitol – citric acid mixtures in the 2600 – 3800 cm^{-1} region are plotted for various compositions in Figure 4b. It can be observed that addition of xylitol to citric acid decreases the contribution of the low-wavenumber component. The temperature dependence of the O – H stretching spectrum was analyzed in the amorphous state (glassy and undercooled liquid states) for xylitol and citric acid in order to better describe the contribution of the OH groups involved in H-bonding to the O – H stretching spectrum.

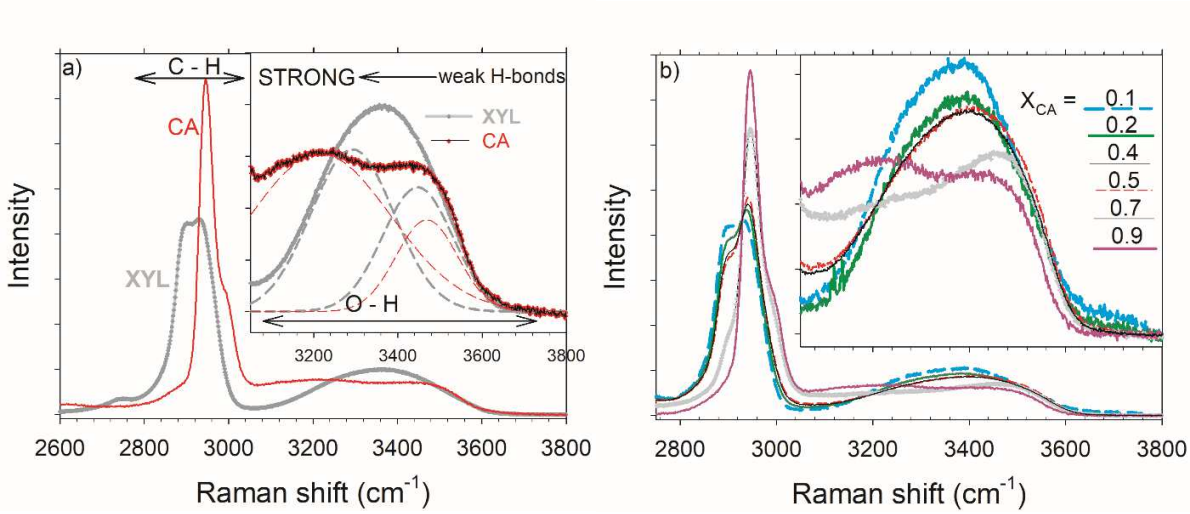

Figure 4: Raman spectra in the C – H and O – H stretching region of a) pure amorphous xylitol and citric acid, b) for various mixtures; the O – H stretching region was enlarged for better clarity

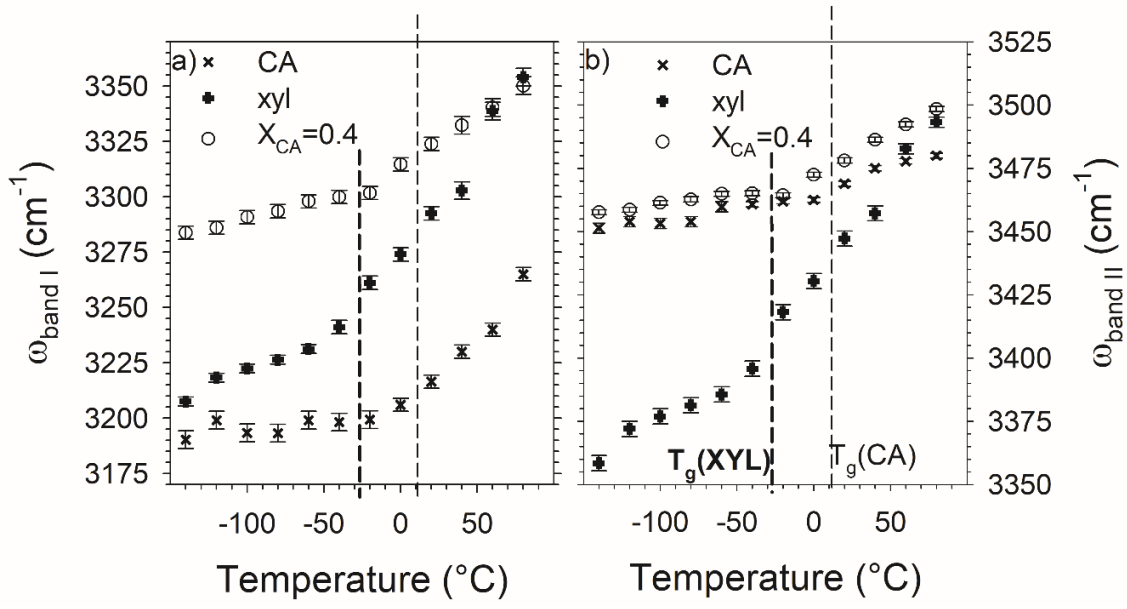

Figure5: wavenumber temperature dependences of the O – H stretching bands I and II for pure xylitol and citric acid and for the eutectic mixture (X_{CA} = 0.4). The dashed lines indicate T_g of pure substances, XYL in thick lines and CA in thin lines.

Using the fitting procedure with 2 Gaussian components described in figure 4a, the wavenumber temperature dependences of the low-wavenumber band (band I) and the high-wavenumber band (band II) were plotted in Figures 5a and 5b respectively. It is clearly observed that the wavenumber of both components increases by temperature increasing, that is the typical signature of OH groups involved in H-bonding[32]. Additionally, the temperature dependences of both

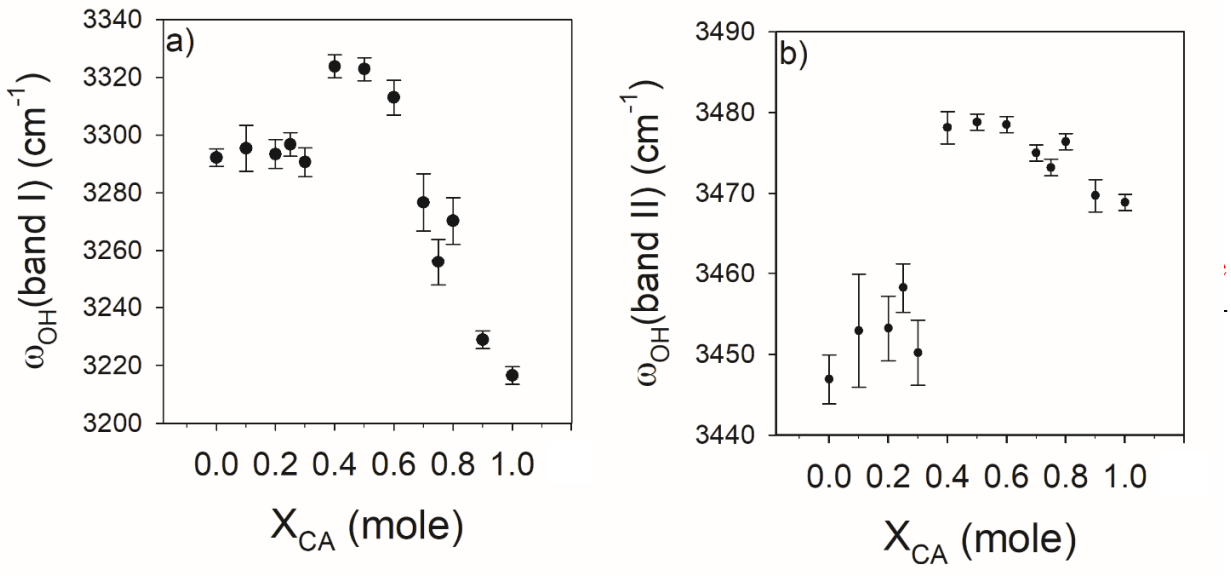

Figure 6: Wavenumber of O – H stretching bands for XYL-CA mixtures, X_{CA} ranging from 0 to 1mole by step of 0.1. Wavenumbers were determined using the fitting procedure described in Fig4a.

observed, reflecting the decreasing of the number of internal O-H…C=O H-bonds. An upshift of band II of CA is also observed by increasing the XYL content, reflecting the homogenization of the strength of H-bonding responsible for the relative sharpening of the O – H stretching spectrum at the eutectic composition. The large distribution of O-H stretching vibrations in CA becomes much narrowed in mixtures of CA content below 0.4 mole. The strong deviation of the experimental liquidus from the predicted liquidus for X_{CA}>0.4 can be associated with the strong wavenumber shift of band I observed by increasing XYL content. Both bands in mixtures composed of less than 0.4 mole of CA have positions similar to those determined in pure xylitol. In this region (X_{CA}<0.4) experimental and predicted liquidus are superimposed, except approaching the eutectic composition at which a discontinuity is observed in the plot of both O – H stretching band positions against X_{CA}. To summarize, the analysis of the O – H stretching spectrum indicates that the origin of the temperature depression of the eutectic point can be interpreted by the disrupting of the H-bond network of CA and the concomitant formation of the supermolecular CA-XYL structure.

3.2.b The C=O stretching spectrum, lying between 1500 and 1900 cm^{-1}, was firstly becomes

becomes much narrowed in mixtures of CA content lower than 0.4 mole. The strong deviation from the ideality observed for X_{CA}>0.4 can be associated with the strong wavenumber shift of band I observed by increasing XYL content. Both bands in mixtures composed of less than 0.4 mole of CA have positions similar to those determined in pure xylitol. In this region (X_{CA}<0.4) mixtures exhibit ideal behavior, except approaching the eutectic composition at which a discontinuity is observed in the plot of both O – H stretching band positions against X_{CA}. To summarize, the analysis of the O – H stretching spectrum indicates that the origin of the temperature depression of the eutectic point can be interpreted by the disrupting of the H-bond network of CA and the concomitant formation of the supramolecular CA-XYL structure.

3.2.b The C=O stretching spectrum, lying between 1500 and 1900 cm^{-1}, was firstly investigated in citric acid at various temperatures, in the amorphous state (glassy and undercooled liquid states), to obtain more detailed information about internal O-H…C=O H-bonds. The spectrum is plotted at 60, 20, and -40 °C in figure 7a. The C=O stretching spectrum is composed of two bands which are clearly temperature dependent. Both bands are shifting toward the high wavenumbers temperature decreasing that is the unambiguous signature of vibrational bands involved H-bonding. The low-wavenumber component (LW) is assigned to intramolecular H-bonds which are stronger than intermolecular interactions and then observed at lower wavenumbers. Interestingly, it is observed that the intensity of the low-wavenumber component of the C=O stretching spectrum decreased at the expense of the high-wavenumber component (HW), as the temperature is decreased. This indicates that the intermolecular H-bonding is promoted by temperature lowering, molecules becoming closer to each other. As a consequence, the number of internal H-bonds decreases by temperature lowering. The C=O stretching spectrum is secondly plotted for various mixtures in Figure 7b.

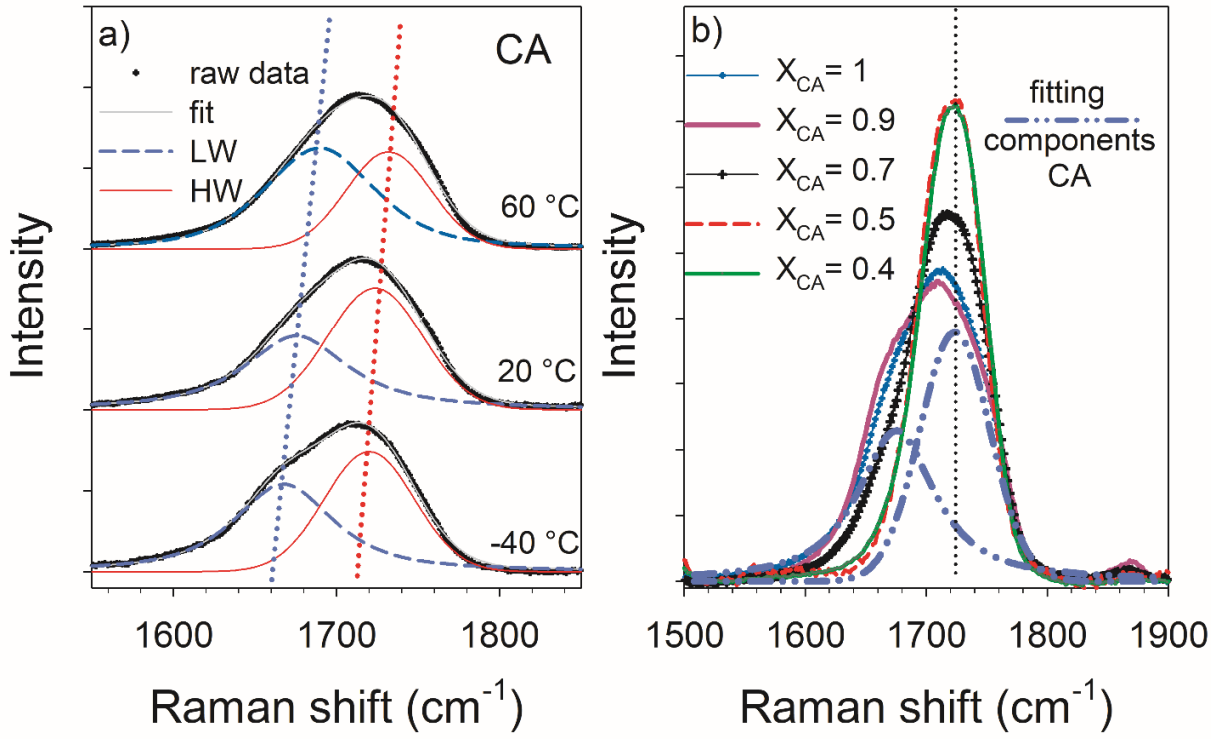

Figure 7: Raman spectrum of the C=O stretching spectrum a) in acid citric at various temperatures, dotted lines being guides for eyes to show the temperature dependence of Raman band positions; b) in various mixtures at

room temperature, peaks in dashed-dotted lines corresponding to the fitting components of the CA spectrum and the vertical dotted line localizing the HW component of CA spectrum.

Figure 7b shows the disappearance of the low-wavenumber component by increasing the xylitol content up to X_{XYL}=0.5-0.6, closely corresponding to the eutectic composition. In this mixture, the C=O stretching spectrum is composed of a single narrow band rigorously corresponding to the high-wavenumber component determined in the fitting procedure of the citric acid spectrum.

Both O-H and C=O stretching vibrations analyzes are converging into a description of the molecular organization in the eutectic mixture as mainly composed of CA-XYL molecular associations in which H-bonding interactions between 2 different and same molecular species have similar strengths.

3.2.c The low-wavenumber analysis can be divided into two parts. Using the data processing described in section2, information on the VDOS of mixtures can be firstly obtained by plotting the Raman susceptibility in figure 2b. The spectra of pure CA and XYL are typical representations of the VDOS of amorphous states without detection of phonon peaks. Both spectra are quite similar and the spectrum of the eutectic mixture (X_{CA}= 0.4). In a second step, the quasielastic intensity is plotted in figure 8b against temperature from spectra collected during a heating ramp at 0.5 °C/min for the mixture X_{CA}=0.1 (figure 8a). $I_{QES}(T)$ is inversely proportional to the temperature dependence of the viscosity. Consequently, this plot gives the opportunity to analyze the phase transformations directly related to an ordering/disordering process, i.e. the glass transition or the recrystallization mechanism from an undercooled liquid state. The glass transition is detected from a change in the slope of $I_{QES}(T)$ in figure 8b, in agreement with several previous analyzes[33-35], and was reported in figure 8c.

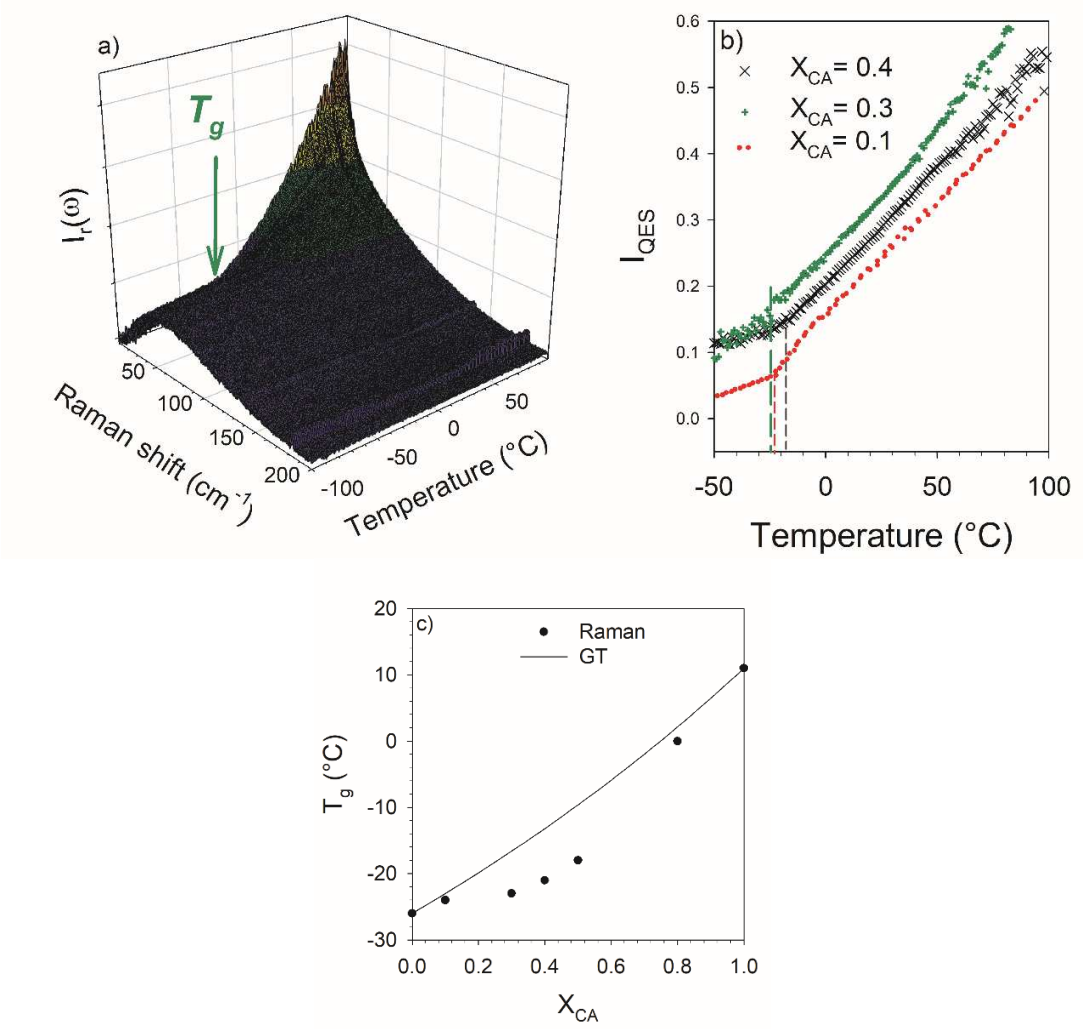

Figure 8 : analysis of the low-wavenumber spectra collected along a heating run at 0.5 °C/min for X_{CA}=0.1; a) spectra are ploted in the reduced intensity representation; b) the quasielastic intensity, obtained by integrating the reduced intensity in the very low-wavenumber region, is plotted against temperature for 3 mixtures. Dashed lines localize T_g for each mixture; c) plot of T_g determined from low-wavenumber analyzes (full circles) and predicted line from Gordon Taylor equation (eq. 3).

The theoretical glass transition can be calculated by the Gordon-Taylor (GT) equation according to[36, 37] :

$$T_g = \frac{(X_{CA}.T_{g,CA}+\kappa.X_{XYL}T_{g,XYL})}{(X_{CA}+\kappa.X_{XYL})} \qquad (3)$$

where X_{CA}, X_{XYL}, $T_{g,CA}$, $T_{g,XYL}$ are molar fractions and glass transition temperatures (K) of citric acid and xylitol respectively, T_g is the theoretical glass transition temperature (K) of mixtures. κ is determined by : $\kappa = T_{g,CA}\rho_{CA}/T_{g,XYL}\,\rho_{XYL}$.

The theoretical T_g curve was also plotted in figure 8c for relevant comparison with experimental values determined from $I_{QES}(T)$ curves. It is worth noting that T_g measured in pure compounds

are found in agreement with the values reported in the literature [38, 39]. In this context, T_g measured in CA indicates the absence of significant amount of water in CA[39]. A deviation of experimental T_g from the GT curve is observed for mixtures with composition close to the eutectic point. Such a behavior has been interpreted in different ways [40-42], including the consideration of the nature of intermolecular H-bonding. Obviously, the present case can be explained from the consideration of a supramolecular structure characterized by medium H-bonding strength, inherent to the disruption of the H-bond network formed either by CA or XYL molecules. It is observed in Figure 5 that the temperature dependences of O – H stretching positions in pure substances exhibit breaks located slightly lower than T_g. This indicates a clear correlation between intermolecular H-bond forces and the molecular mobility. Given that H-bonding interactions are weaker in the eutectic mixtures compared to those in pure substances, the deviation of T_g from the GT line around the eutectic composition can be explained by a more flexible H-bond network in the supramolecular structure compared to H-bond networks in CA and XYL.

3.3. Dissolution of active pharmaceutical ingredients (APIs) in CA-XYL mixtures

Ibuprofen (IBP) and paracetamol have been dissolved in the eutectic mixture. There were selected because of their poor water-solubility (0.043 $mg.ml^{-1}$ at 37 °C for IBP, and 1g/100g 10$mg.ml^{-1}$at 20 °C for PARA). Additionally, as-received IBP and PARA crystalline powders melt at very different temperatures (T_m(IBP) ~ 76 °C, T_m(PARA) ~ 170 °C). Both APIs were dissolved in DES in the same conditions (T ~ 80°C) in the liquid eutectic mixture. It can be outlined that IBP is in the liquid state at 80 °C, while crystalline powder of paracetamol was dissolved in DES at this temperature.

After dissolution IBP-S at 80 °C, mixtures were cooled down to -100 °C for a low-wavenumber in-situ analysis upon heating at 0.5 °C/min. Spectra were firstly collected at -100 °C for checking the absence of phonon peaks i.e. the amorphous form of the formulation. Spectra were collected in the same conditions for IBP-S, CA-XYL (X_{CA}= 0.4), and IBP-S(20 wt%)CA(0.4)-XYL. Using the same data processing method (experimental section), for the various data sets, the quasielastic intensity (I_{QES}) was plotted against temperature in figure 9a. The I_{QES}(T) plot for IBP-S clearly shows the glass transition at T_g ~ -50 °C as expected[34], via a change in the slope, the recrystallization directly in the stable form (by contrast to the racemic form[34, 43]) at about 5 °C via a considerable decrease of I_{QES}, and the melting of the stable form at 50 °C via the increase of I_{QES} which has the same temperature dependence as in the undercooled liquid. For the eutectic mixture, the I_{QES}(T) plot only reveals the glass transition at T_g ~ -22 °C without any signature of recrystallization. The I_{QES}(T) plot for the formulation containing 20% of IBP-S is quasi superimposed with that of pure IBP-S except around T_g. The slope breaking corresponding to the glass transition is less marked in the formulation and T_g located at higher temperature than in pure IBP-S. The important information is that a considerable amount of IBP-S (20 wt%) can be dissolved in the eutectic CA(0.4)-XYL mixture with no signature of recrystallization in a large temperature range [-100 °C; 80 °C].

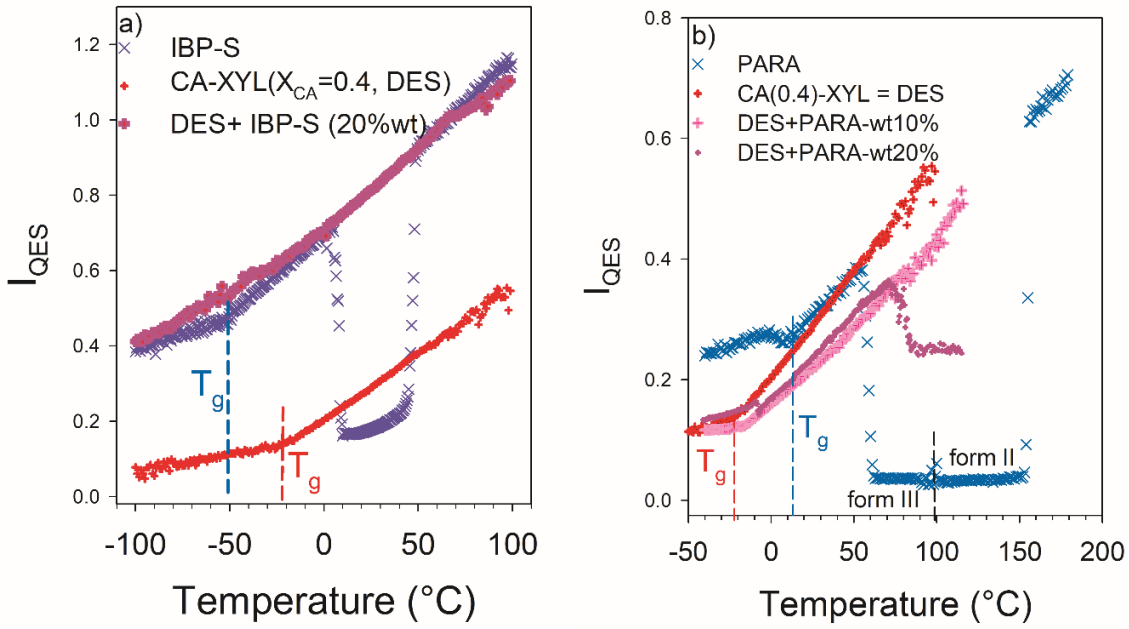

Figure9: temperature dependence of the quasielastic intensity, for IBP-S, the CA-XYL eutectic mixture (X_{CA}=0.4, ES) and a) the formulation DES+IBP-S(20 wt%); b) the formulations DES+PARA-S(10 wt%, 20 wt%)

The dissolution of crystalline paracetamol was performed in the same conditions as for IBP, and the formulation was then cooled down to -40 °C for the in-situ analysis upon heating up to 115 °C. The comparison of temperature dependence of the quasielastic intensity determined upon heating PARA, the eutectic mixture (DES) and two formulations of PARA was plotted in figure 9b. The I_{QES} plot of paracetamol provides the complete sequence of phase transformation including the polymorphic III→II phase transformation detected around 100 °C via a subtle discontinuity of the quasielastic intensity. As for IBP, the absence of phonon praks after cooling was checked indicating the absence of crystallites in PARA. The I_{QES} plot of the formulation composed of 20 wt% of PARA shows a depressed T_g reflecting the plasticizing effect of the eutectic mixture on PARA. Additionally, the recrystallization of PARA dissolved in DES is detected at temperature slightly higher than the temperature of recrystallization of pure PARA. However, the value of I_{QES} significantly higher in the formulation than in the crystalline state of PARA suggests an incomplete crystallization of PARA in the formulation. The low-wavenumber spectrum of the formulation containing 20 wt% of PARA collected after recrystallization was compared to spectra of the various forms of PARA in figure 10 for identifying the recrystallized form. This figure clearly reveals amorphous PARA into a very poorly crystallized form I in the formulation, while pure PARA recrystallized in form III. The very low degree of crystallization determined upon heating the formulation is consistent with of great values of the quasielastic intensity calculated after recrystallization (see I_{QES}(T) plot in Figure 10), induced by the

amorphous contribution of the amorphous solvent and the low degree of crystallization in form I. A formulation containing 10 wt% of PARA was then analyzed in the same conditions and the $I_{QES}(T)$ plot was reported in Figure 9b. The enhancement of the plasticizing effect of the eutectic mixture on PARA is firstly observed via a lower T_g than in the formulation containing 20 wt% of PARA. Secondly, no trace of crystallization of PARA was detected in the -40 – 115 °C temperature range.

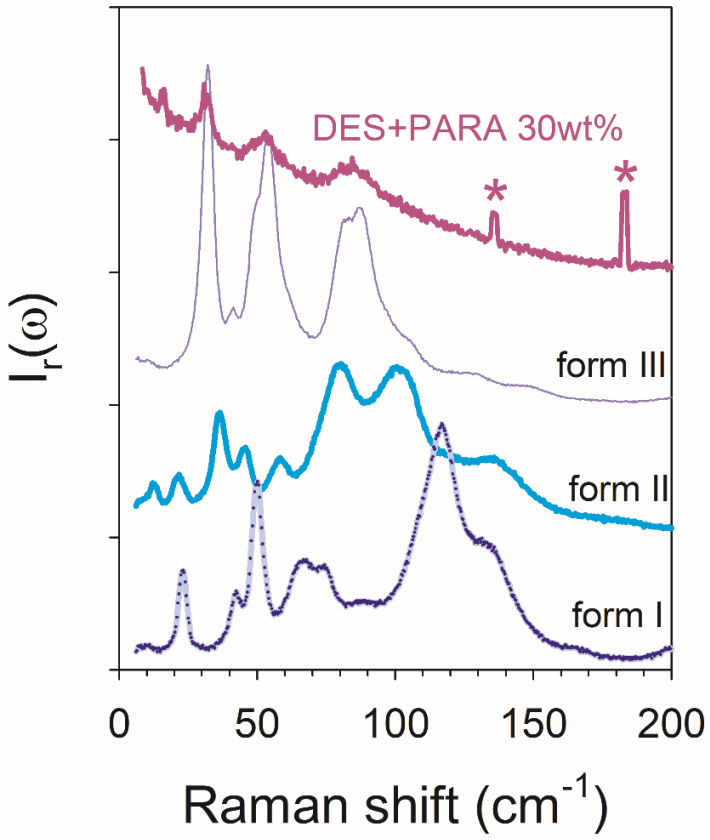

Figure10: low-wavenumber spectrum of polymorphic forms of paracetamol compared to the formulation containing 20 wt% of paracetamol. Spectra were taken at room temperature. Stars localize laser lines.

4. Conclusion

The present study reports the determination of the equilibrium phase diagram of the CA-XYL system performed at the same time as Raman investigations of molecular associations via H-bonding. It was found that the drastic negative deviation from ideality observed for high CA content is mainly associated with the formation of molecular associations between CA and XYL. Low-wavenumber Raman spectroscopy was used for determining T_g of mixtures and for

monitoring the physical stability of APIs dissolved in the eutectic mixture. This study reveals that a great amount of ibuprofen and paracetamol (20wt%) can be dissolved in the eutectic mixture, while they are considered as poorly water-soluble model drugs. In the case of the PARA formulation the drug recrystallizes in a very poorly crystallized form II, while pure PARA usually recrystallizes in form III. This indicates that DES can be used to stabilize a great amount of amorphous of APIs and to prepare unusual crystalline forms of APIs.

References

[1] C. Leuner, J. Dresmann, Eur. J. Pharm. Biopharm. 50 (2000) 47.
[2] G. Van den Mooter, Drug Discovery Today: Technologies 9 (2012) e79.
[3] P.J. Marsac, S.L. Shamblin, L.S. Taylor, Pharm. Res. 23 (2006) 2417.
[4] J.W. Steed, Trends Pharmacol. Sci. 34 (2013) 185.
[5] N. Chieng, J. Aaltonen, D. Saville, T. Rades, Eur. J. Pharm. Biopharm. 71 (2009) 47.
[6] R. Laitinen, K. Lobmann, C.J. Strachan, H. Grohganz, T. Rades, Int. J. Pharm. 453 (2013) 65.
[7] E. Juere, F. Kleitz, Microporous Mesoporous Mater. 270 (2018) 109.
[8] I.M. Marrucho, L.C. Branco, L.P.N. Rebelo, Annu. Rev. Chem. Biomol. Eng. 5 (2014) 527.
[9] N. Adawiyah, M. Moniruzzaman, S. Hawatulaila, M. Goto, Med. Chem. Comm. 7 (2016) 1881.
[10] M. Moniruzzaman, M. Tamura, Y. Tahara, N. Kamiya, M. Goto, Int. J. Pharm. 400 (2010) 243.
[11] M.J. Earle, J. Esperança, M.A. Gilea, K.R. Seddon, J.A. Widegren, Nature 439 (2006) 831.
[12] A. Abbott, D. Boothby, G. Capper, D. Davies, R. Rasheed, J. Am. Chem. Soc. 126 (2004) 9142.
[13] E. Smith, A. Abbott, K. Ryder, Chem. Rev. 114 (2014) 11060.
[14] M. Martins, S. Pinho, J. Coutinho, J. Solution Chem. 48 (2019) 962.
[15] H. Morrison, C.C. Sun, S. Neervannan, Int. J. Pharm. 378 (2009) 136.
[16] R. Craveiro, I. Aroso, V. Flammia, T. Carvalho, M. Viciosa, M. dioniisio, S. Barreiros, R. Reis, A. duarte, A. Paiva, J. Mol. Liq. 215 (2016) 534.
[17] D. Abranches, M. Martins, L. Silva, N. Schaeffer, S. Pinho, J. Coutinho, Chem. Commun. 55 (2019) 10253.
[18] Y. Dai, J. van Spronsen, G. Witkamp, R. Verpoorte, Y. Choi, Anal. Chim. Acta 766 (2013) 61.
[19] T. Phaechamud, S. Tuntarawongsa, P. Charoensuksai, AAPS Pharm Sci Tech 17 (2015) 1213.
[20] A. duarte, A. Ferreira, S. Barreiros, E. Cabrita, R. Reis, A. Paiva, Eur. J. Pharm. Biopharm. 114 (2017) 296.
[21] M. Elbagerma, H.G.M. Edwards, T. Munshi, I.J. Scowen, Cryst. Eng. Comm. 13 (2011) 1877.
[22] K. Shimono, K. Kadota, Y. Tozuka, A. Shimosaka, Y. Shirakawa, J. Hidaka, Eur. J. Pharm. Sci. 76 (2015) 217.
[23] A. Hédoux, Y. Guinet, M. Descamps, Int. J. Pharm. 417 (2011) 17.
[24] A. Hédoux, Adv. Drug Deliv. Rev. 100 (2016) 133.
[25] F.L. Galeener, P.N. Sen, Physical Review B 17 (1978) 1928.
[26] R. Shuker, R. Gammon, Physical Review Letters 25 (1970) 222.
[27] J. Coutinho, S. Andersen, E. Stenby, Fluid Phase Equilib. 103 (1995) 23.
[28] M. Karimi-Jafari, L. Pradela, G. Walker, D. Croker, Cryst. Growth Des. 18 (2018) 6370.
[29] G.-C. Zhang, H. Lin, S. Lin, J. Pharm. Biomed. Anal. 66 (2012) 162.
[30] S. Rehder, M. Klukkert, K. Lobmann, C. Strachan, A. Sakmann, K. Gordon, T. Rades, C. Leopold, Pharmaceutics 3 (2011) 706.
[31] P. Stott, A. Williams, B. Barry, J. Control. Release 50 (1998) 297.
[32] A. Hédoux, Y. Guinet, L. Paccou, P. Derollez, F. Danede, J. Chem. Phys. 138 (2013) 214506.
[33] Y. Guinet, L. Paccou, F. Danede, J.F. Willart, P. Derollez, A. Hédoux, Int. J. Pharm. 509 (2016) 305.
[34] B. Malfait, L. Paccou, P. derollez, Y. Guinet, A. Hedoux, J. Raman Spectr. 50 (2019) 1027.
[35] Y. Guinet, L. Paccou, F. Danede, P. derollez, A. Hédoux, Int. J. Pharm. 526 (2017) 209.
[36] Q. Lu, G. Zografi, Pharmaceutical research 15 (1998) 1202.
[37] A. Forster, J. Hempenstall, I. Tucker, T. Rades, Dev. Ind. Parm. 27 (2001) 549.
[38] K. Elamin, J. Sjostrom, H. Jansson, J. Swenson, J. Chem. Phys. 136 (2012) 104508.
[39] L. Lu, G. Zografi, J. Pharm. Sci. 86 (1997) 1374.
[40] L. Weng, G. Elliot, Pharm. Res. 32 (2015) 2217.
[41] V.d. Sman, J Phys Chem B 117 (2013) 16303.

[42] W.F. Wolkers, A.E. Oliver, F. Tablin, J.H. Crowe, Carbohydr. Res. 339 (2004) 1077.
[43] A. Hédoux, Y. Guinet, P. Derollez, E. Dudognon, N. Correia, Int. J. Pharm. 421 (2011) 45.

Negative deviation from ideality ← Decreased OH…O forces